Applied Clay Science 45 (2009) 194–200

Contents lists available at ScienceDirect

Applied Clay Science

journal homepage: www.elsevier.com/locate/clay

Hematite and iron carbonate precipitation-coexistence at the iron–montmorillonite–salt solution–CO_2 interfaces under high gas pressure at 150 °C

G. Montes-Hernandez [a,*], J. Pironon [b]

[a] University Joseph Fourier, Laboratoire de Planétologie de Grenoble, Observatoire des Sciences de l'Univers de Grenoble and CNRS/INSU, BP 53, 38041 Grenoble Cedex 9, France
[b] Henri Poincaré University, CNRS, UMR G2R, BP 239, 54506 Vandoeuvre lès-Nancy, France

ARTICLE INFO

Article history:
Received 27 February 2009
Received in revised form 29 May 2009
Accepted 8 June 2009
Available online 13 June 2009

Keywords:
Dissolution
Precipitation
Montmorillonite
Nanoparticles
Hematite–iron carbonate
Carbon dioxide

ABSTRACT

The hydrothermal reactivity of swelling clays has relevant implications on the geological storage of radioactive waste and greenhouse gases because the clay geo-materials have been proposed as engineered or natural barriers due to their low permeability in confined systems and their high capacity to sequester ions. In the present study, the iron–montmorillonite–salt solution–CO_2 interactions were investigated under high gas pressure (200 bar) at 150 °C.

Various chemical processes were characterized at the solid–fluid interfaces such as the dissolution of montmorillonite fine particles and oxidative-dissolution of elemental iron. The ionic supersaturation of solution and possibly the surface complexation in the system produced the precipitation of hematite nanoparticles (<200 nm) after 15 days of solid–fluid contact. The hematite nanoparticles dispersed and/or coagulated on the clay matrix caused a stable red coloration of the montmorillonite composite. We assume that initial dissolved oxygen was progressively consumed in this closed-stirred system favouring the presence of divalent iron (in-situ change of redox conditions) and then leading the surface precipitation of iron carbonate nanocrystals (<500 nm) after 60 days of solid–fluid contact. Thus, an atypical mineral coexistence of hematite–iron carbonate was observed in our system. A qualitative comparison with the blank experiment, i.e. at the same *P–T* conditions, but without CO_2 injection, suggested that the carbon dioxide increased the hydrothermal reactivity of montmorillonite because the hematite and iron carbonate formation were not observed after the same reaction time.

1. Introduction

The physicochemical reactions at solid/fluid interfaces play a crucial role in the global cycle of major and traces elements. Experimental and numerical simulation of these reactions is important to understand and predict the fate and transport of chemical elements in natural and artificial environments. Obviously, the fate and transport of chemical elements are controlled by their chemical form and speciation. These processes are closely linked with the physicochemical and textural properties of porous media such as porosity, specific surface area, mineral composition, hydrothermal or aqueous reactivity, surface charge, reactive surface area, mineral chemical stability, swelling, etc. Fate and transport of chemical elements can be significantly associated to transport of colloidal and dispersed matter such as nanominerals, mineral nanoparticles, nanocomposites, bacteria, etc. (Steefel and Van Cappellen, 1990; Charlet and Manceau, 1994; Manceau and Charlet, 1994; Steefel and Van Cappellen, 1998; Sigg et al., 2000; Montes et al., 2005; Wood et al., 2007; Hochella et al., 2008 and others). Consequently, the physicochemical reactions at solid–fluid interfaces have considerable importance in the ecological, geochemical, biological, planetological and industrial area (Fig. 1).

The present experimental study was focussed on the hydrothermal reactivity of Ca-montmorillonite in the presence of supercritical carbon dioxide; this having relevant implications on the geological sequestration of CO_2. The increasing atmospheric CO_2 concentration, mainly caused by fossil fuel combustion, has led to concerns about global warming. A partial regulation of the balance of carbon dioxide within the atmosphere (an integral component of the carbon cycle) is controlled by equilibrium cycling between mineralised carbonates and atmospheric carbon dioxide (Dickinson et al., 2002). A possible technology that can contribute to the reduction of carbon dioxide emissions is the geological sequestration of CO_2 and the ex-situ mineralization of CO_2 (controlled industrial reactors), and the latter possibility was originally proposed by Seifritz (1990) and first studied in more detail by Lackner et al. (1995). For these arguments, it is essential to study in detail the physicochemical effect of CO_2 on the geo-materials.

For long-term geological sequestration of CO_2, the ability of the cap rock (shale or mudstone) to seal fluids and/or to sequester ion aqueous species is one of the most important factors. In this context, it

* Corresponding author.
E-mail addresses: german_montes@hotmail.com, german.montes-hernandez@obs.ujf-grenoble.fr (G. Montes-Hernandez).

0169-1317/$ – see front matter © 2009 Elsevier B.V. All rights reserved.
doi:10.1016/j.clay.2009.06.004

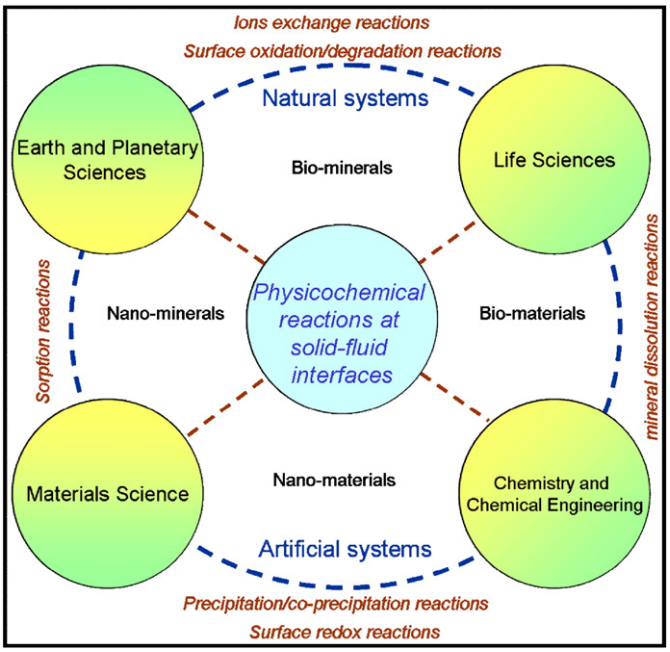

Fig. 1. Schematic representation of relevance of physicochemical reactions at solid–liquid interfaces in natural and artificial systems, including some examples.

is also essential to have a good understanding of the effect of the equilibrium ($CO_{2(aq)} + 2H_2O \Leftrightarrow HCO_3^- + H_3O^+$) on the cap rock, particularly, on the swelling clay minerals, which are considered as natural or engineered buffer barriers for waste storage. Shale or marls are clay-rich materials with a complex mineral composition, and frequently, the presence of no-clay minerals and/or accessory minerals makes the understanding of their physicochemical reactivity difficult. For this reason, in this preliminary experimental investigation, a homoionic calcium montmorillonite purified and separated from the Wyoming bentonite (labelled Wy2) was used. Herein, various analytical techniques were used to characterize solid samples (SEM/EDS, TEM/EDS and infrared microscopy) and solution samples (ICP-AES).

2. Materials and methods

2.1. Homoionic calcium montmorillonite

An amount of 40 g of Wyoming bentonite was dispersed into 1 L of high-purity water with electrical resistivity of 18.2 MΩ cm; this dispersion was kept in constant mechanical agitation at 25 °C and adjusted at pH = 5 with acid acetic. Then, the suspension was heated at 80 °C during 8 h in order to eliminate the carbonates. The solid phase was recuperated by centrifugation (45 min at 13,000 rpm) and re-dispersed in 1 M $CaCl_2$ solution and kept in constant mechanical agitation for 24 h at 25 °C. Then, the solid was separated by centrifugation (45 min at 13,000 rpm), and the supernatant solution was decanted. This process was repeated three times. The associated minerals (quartz, feldspar, etc.) were manually separated after each centrifugation.

The purified Ca-montmorillonite was washed several times with high-purity water until the $AgNO_3$ test for chloride was negative. This purified bentonite was dried for 48 h at 60 °C and gently ground in a mortar.

The transmission electron microscopy (TEM) coupled to energy dispersive X-ray analyser was used to determine the homoionic interlayer cation in the montmorillonite particles. Herein, the structural formula of Ca-montmorillonite $[Si_{3.90}Al_{0.10}O_{10}(OH)_2](Al_{1.54}Fe^{III}_{0.22}Mg_{0.19})Ca_{0.22}$ was calculated from 10 particles EDS-TEM analysis according to the method of Harvey (1943), i.e. on the basis of 11 oxygen for particles of 2:1 clay minerals. Recent studies showed that the structural iron in the montmorillonite from Wyoming is partially oxidized; reported about 50% Fe^{2+} and 50% Fe^{3+}. The purification of the Wyoming bentonite was carried out in the LEM laboratory (INPL-Nancy).

2.2. Experiments of solid–fluid interactions

100 ml salt solution (0.5 M of NaCl) and 3 g of Ca-montmorillonite were charged in the reactor (engineer autoclave with internal volume of about 200 ml). The montmorillonite particles were immediately dispersed with magnetic agitation (500 rpm). The dispersion was then saturated with CO_2 gas at 20 °C and 50 bar, using an injection system in the reactor. The pressure drop due to absorption-dissociation into dispersion was compensated by various manual CO_2 injections until pressure equilibration (about 48 h), under these conditions where 13.5 g of total CO_2 was injected in the system (4.5 g of CO_2 trapped into dispersion). Then, heating and argon injection were carried out to adjust the pressure and temperature at 200 bar and 150 °C, respectively. These *P–T* conditions have been chosen to fit with conditions of CO_2 storage in deep depleted reservoirs. Two different durations of reaction were considered (15 and 60 days). Finally, in order to evaluate the effect of CO_2, a blank experiment was carried out at the same temperature–gas pressure conditions for a duration of 15 days, without CO_2 injection in the system; i.e. 200 bar of pressure was reached only with argon gas. The three experiments were labelled CO_2-Argon_15, CO_2-Argon_60 and Argon-blank.

Previous experiments of solid–fluid interactions under high gas pressure and temperature in the presence of supercritical CO_2 revealed a slight corrosion of the wall of the Hastelloy B-2 reactor and magnetic agitator, both protected with Teflon material. This corrosion produced a continuous iron source into the system. This technical problem was used here as non-controlled iron source in the experiments.

After 15 and 60 days, the autoclave was removed from the heating system and immersed in cold water. The depressurization of reaction cell was carried out after immersion in cold water. The autoclave and reaction cell were disassembled at about 30 °C, and the solid product was separated by centrifugation (15 min at 13,000 rpm) and decanting of the supernatant solutions. These operating activities were conducted in a period of less than 2 h.

Finally, the solid product was washed by dispersion-centrifugation several times with high-purity water until the $AgNO_3$ test for chloride was negative. The washed product was dried for 48 h at 60 °C and gently ground in a mortar.

2.3. Analytic procedures

2.3.1. Microscopic observations and EDS microanalyses

Morphological analyses of solid samples (powders) were performed by scanning electron microscopy (SEM), using a HITACHI S-4800 microscope. Isolated fine particles (oriented on carbon Ni grids) of the starting and reacted samples were also studied using a JEOL 3010 transmission electron microscope (TEM) equipped with an energy dispersive X-ray analyzer (EDS).

2.3.2. Infrared measurements

An infrared micro-imaging spectrometer (BRUKER HYPERION 3000) coupled with an environmental reaction cell was used in transmission mode, with an MCT mono-detector at 4 cm^{-1} resolution for 100 scans. The typical size of the infrared spot onto the sample was ~50 × 50 μm^2. For these measurements, a sample (powder) containing iron carbonate was manually deposited and compressed as a thin film on a KBr window. The KBr window was carefully placed in an environmental reaction cell in order to measure the iron carbonate thermo-reactivity using vacuum drying at 300 °C. This experimental instrument is available in the LPG laboratory (OSUG-Joseph Fourier University in Grenoble).

Table 1
Major ion concentrations in the interacting solution for three experiments measured by ICP-AES.

Experiment	Duration (days)	Major ion concentration (mg/L)						
		Si	Fe	Mg	Ca	Na	K	Al
Argon-blank	15	78.60	<DL	13.80	448.00	10,273	<DL	8.83
CO_2-Argon_15	15	47.10	<DL	<DL	274.80	10,463	16.70	10.51
CO_2-Argon_60	60	87.20	<DL	18.00	529.60	11,536	19.90	16.10

2.3.3. ICP spectrometry

The aqueous solutions were filtered through a 0.02-μm Teflon filter and immediately acidified with nitric acid solution (1% v/v) for measurements of major cations (Al, Ca, Mg, Na, Fe and Si) by inductively coupled plasma atomic emission spectrometry (ICP-AES Jobin-Yvon JY 70).

3. Results and discussion

Various physicochemical processes were characterized at the iron–montmorillonite–salt solution–CO_2 interfaces such as the cation exchange process on the clay mineral particles, the dissolution of the most fine montmorillonite particles and oxidative-dissolution of elemental iron. The ionic supersaturation into the interacting solution due to dissolution processes led to the precipitation of hematite nanoparticles (<200 nm) after 15 days of solid–fluid contact and later the precipitation of iron carbonate nanocrystals (<500 nm) after 60 days of solid–fluid contact. The description of these reaction mechanisms is explained in the following paragraphs.

3.1. Cation exchange

The high concentration of Na^+ in the solution (0.5 M) led to cation exchange on the clay mineral particles. EDS-TEM analyses showed that about 60% of initial calcium was exchanged by sodium after 15 days. A similar process was also observed in the blank experiment. Thus, the cation exchange process was independent of the CO_2 injection, i.e., the cation exchange process was independent of the pH of interacting solution. The cation exchange process can be represented by the following chemical reaction:

$$[Si_{3.90}Al_{0.10}O_{10}(OH)_2](Al_{1.54}Fe^{III}_{0.22}Mg_{0.19})Ca_{0.22} + 0.26Na^+ \leftrightarrow [Si_{3.90}Al_{0.10}O_{10}(OH)_2](Al_{1.54}Fe^{III}_{0.22}Mg_{0.19})Na_{0.26}Ca_{0.09} + 0.13Ca^{+2}.$$

3.2. Dissolution process of fine montmorillonite particles

The concentration increase in the solution of silica (from 9 to 87 mg/L), magnesium (from <DL to 18 mg/L) and calcium (from 12 to 530 mg/L) after 60 days of solid–fluid interaction, confirmed the dissolution process of montmorillonite particles. The major ion concentrations in the interacting solution for three experiments are reported in Table 1. We assume for the closed-stirred system with high liquid–solid ratio (33.33 g/g), the most fine montmorillonite particles were firstly dissolved because the micro-chemical (EDS-TEM) analyses revealed a similar elemental composition for starting and reacted clay particles. The dissolution process of fine-clay particles can be then described by:

$$[Si_{3.90}Al_{0.10}O_{10}(OH)_2](Al_{1.54}Fe^{III}_{0.22}Mg_{0.19})Ca_{0.22} + 6.4H^+ \Rightarrow 3.90SiO_{2(aq)} + 1.64Al^{+3} + 0.22Fe^{+3} + 0.19Mg^{+2} + 0.22Ca^{+2} + 4.2H_2O.$$

Note that the quantification of montmorillonite dissolution extent with time in the closed system is difficult because the liberated major ions are susceptible to form other mineral phases or coagulate colloidal matter. This was the case for silica, aluminium and iron (see following paragraphs). The calcium cannot be selected as dissolution tracer because it was also an exchangeable ion in our system. Conversely, the magnesium ion could be a reliable dissolution tracer at 60 days of solid–fluid interaction because this ion was not detected in the formed nanoparticles. Herein, the dissolution of montmorillonite was estimated to be 4% using the magnesium concentration as dissolution tracer after 60 days of solid–fluid interaction (18 mg/L, Table 1) and EDS analyses for magnesium in starting montmorillonite particles (average mass percent = 1.48%).

3.3. Hematite precipitation

The red stable coloration of product suggested an oxidative-dissolution of elemental iron and/or a dominant presence of Fe^{3+} into the system. Moreover, The EDS-TEM analyses (Table 2) and the TEM observations showed fine spherical particles (<200 nm) of iron oxide (hematite type) dispersed and/or coagulated in the montmorillonite after 15 days of solid–fluid contact (Fig. 2). For this case, the heterogeneous nucleation/precipitation process of iron oxide nanoparticles can be described as follows (Montes-Hernandez et al., 2006):

$$2Fe^{+3} + 9H_2O \rightarrow Fe_2O_3 + 6H_3O^+ (\text{at } T>125^{\circ}C).$$

Note that the EDS-TEM analyses (Table 2) revealed also an association of silica and aluminium with formed iron oxide nanoparticles. To explain this association, a coagulation process of colloidal clay mineral particles is suggested by dissolved iron and/or clusters of iron oxide. Another explanation could be the iron oxide nucleation in the clay mineral particle and then a progressive liberation of structural silica and aluminium. This hypothesis is supported by Fig. 3, showing the silica–aluminium distribution in montmorillonite particles and in/on iron oxide nanoparticles at 15 and 60 days of solid–fluid

Table 2
EDS-TEM analyses in the iron oxide nanoparticles synthesized under hydrothermal conditions.

Analysis	Mass percent for elements in iron oxide nanoparticles							Observation
	Fe	O	Na	Mg	Ca	Al	Si	
Reference	69.94	30.05	00.00	00.00	00.00	00.00	00.00	Hematite composition
1	62.72	32.18	00.07	00.00	00.10	01.89	03.03	Reaction time: 15 days
2	61.88	31.52	00.00	00.00	00.33	01.82	04.45	Reaction time: 15 days
3	57.96	34.16	00.64	00.00	00.25	02.20	04.78	Reaction time: 15 days
4	60.67	32.97	00.00	00.07	00.31	01.97	04.00	Reaction time: 15 days
5	64.01	32.84	00.00	00.00	00.16	0.62	02.37	Reaction time: 15 days
Average	61.44	32.73	00.14	00.01	00.23	01.70	03.72	Average composition for iron oxide nanoparticles
1	67.40	30.30	00.00	00.00	00.00	00.53	01.76	Reaction time: 60 days
2	70.21	28.56	00.00	00.00	00.00	00.50	00.73	Reaction time: 60 days
3	64.22	31.25	00.00	00.00	00.26	01.56	02.72	Reaction time: 60 days
Average	67.27	30.03	00.00	00.00	00.08	00.86	01.73	Average composition for iron oxide nanoparticles

The average element composition was similar to hematite mineral, particularly the iron oxide produced after 60 days of reaction time.

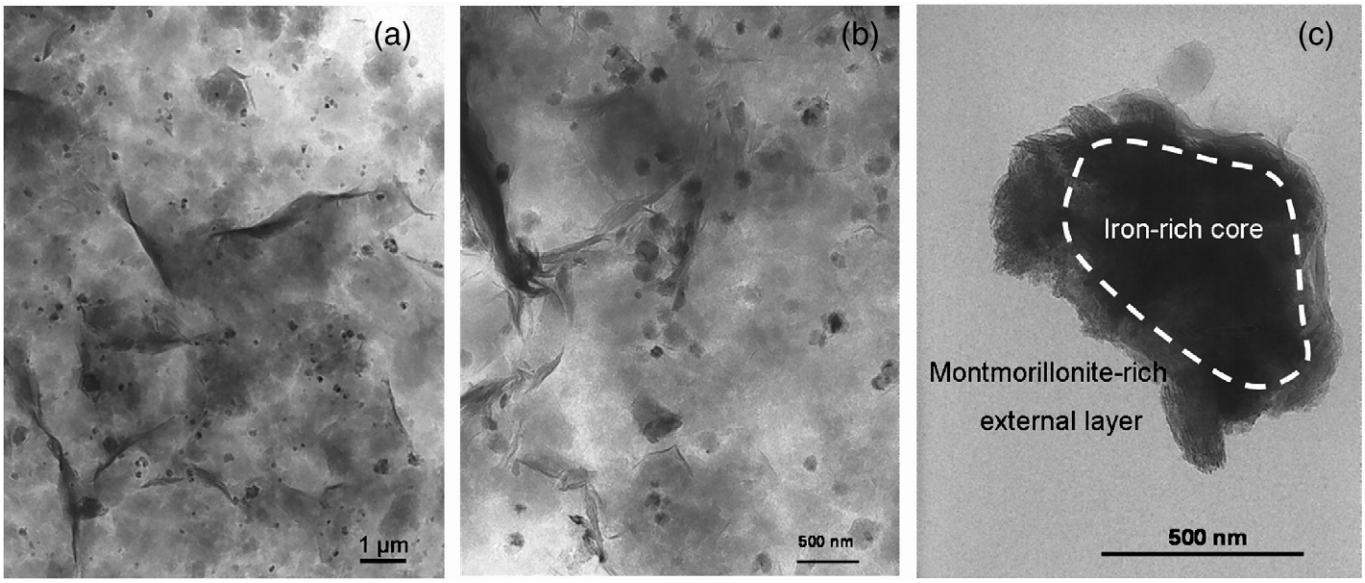

Fig. 2. TEM observations for reacted montmorillonite sample after 15 days of solid–fluid contact. (a) and (b) Spherical nanoparticles of hematite (<200 nm) dispersed and/or coagulated in the montmorillonite matrix. (c) Fine particle with iron-rich core and montmorillonite rich external layer.

interaction. Unfortunately, the MET observations showed an unclear effect of duration reaction on the particle size of iron oxide. The iron oxide nanoparticles were not detected by X-ray diffraction (laboratory X-ray source) (Montes-Hernandez et al., 2006), possibly due to their poor crystallinity, small size and/or low content in the clay mineral.

3.4. Iron carbonate precipitation

For the long-term experiment (60 days of solid–fluid contact), the TEM observations and EDS-TEM analyses indicated the iron carbonate precipitation. The rhombohedral nanocrystals (<500 nm) of iron carbonate were clearly observed (Fig. 4). In terms of chemical composition, two types of iron carbonate were characterized; the iron carbonate (type siderite) and a complex iron–nickel–cobalt carbonate solid solution (Table 3). The cobalt–iron–nickel presence in the carbonates came from the reactor alteration as mentioned above. The Co–Fe–Ni distribution in the carbonates is reported in a ternary graph (Fig. 5). This figure showed clearly the presence of other iron sources in our experiments. These unpredicted data demonstrate that toxic ions can be adsorbed and/or incorporated on/in carbonates during a given carbonation process (Montes-Hernandez et al., 2009).

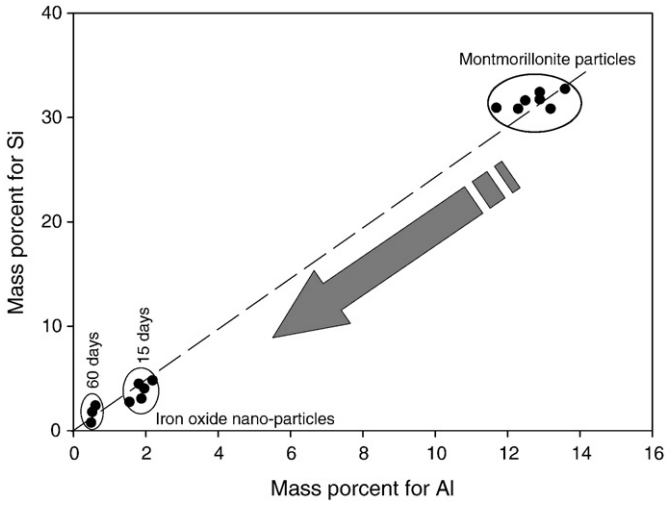

Fig. 3. The silica–aluminium distribution in starting montmorillonite particles and in/on iron oxide nanoparticles formed at 15 and 60 days of solid–fluid interaction. Microchemical EDS-TEM analyses.

The iron carbonate characterization was supported by infrared measurements. The CO_3-stretching vibration band (ν_3) at 1464 was clearly identified on the reacted montmorillonite sample. The CO_3-stretching vibration band for iron carbonates was slightly shifted with respect to CO_3-stretching vibration band at 1454 for pure calcite. The other vibration bands (ν_1, ν_2 and ν_4) for iron carbonates were not clearly observed. The in-situ vacuum drying of montmorillonite revealed that the contained carbonate was thermally stable up to <300 °C, thermal decomposition of carbonate and complete water desorption from montmorillonite were observed at 300 °C during 5 h under dynamic vacuum (1 mbar) (Fig. 6).

Iron carbonate precipitation suggests an in-situ change of redox conditions, producing such an atypical hematite–iron carbonate coexistence after 60 days of solid–fluid interaction. This mineral coexistence was not observed after 15 days. We assume that initially dissolved oxygen was progressively consumed favouring the presence of divalent iron (Fe^{2+}). For example, the siderite precipitation can be then represented as follows:

$$Fe^{2+} + 2HCO_3^- \leftrightarrow FeCO_{3(s)} + H_2O + CO_2.$$

In our experiments, the iron ion was significantly substituted by cobalt and nickel ions during carbonation process.

3.5. Complementary comments

The silica liberated into the solution by dissolution of fine montmorillonite particles led to the micro-particle precipitation (<5 µm) of silica as supported by TEM observations.

EDS-TEM analyses showed that silica and aluminium liberated into the solution by the montmorillonite dissolution were always associated to the formation of iron oxides (Fig. 3) and silica in our experiments.

Calcium ions liberated by cation exchange and/or dissolution, and magnesium ions liberated by dissolution, suggest the precipitation of calcium and/or magnesium carbonates when a supersaturation state of interacting solution is reached with respect to the cited carbonates:

$$Ca^{+2} + 2HCO_3^- \rightarrow CaCO_{3(s)} + H_2O + CO_2$$

$$Mg^{+2} + 2HCO_3^- \rightarrow MgCO_{3(s)} + H_2O + CO_2.$$

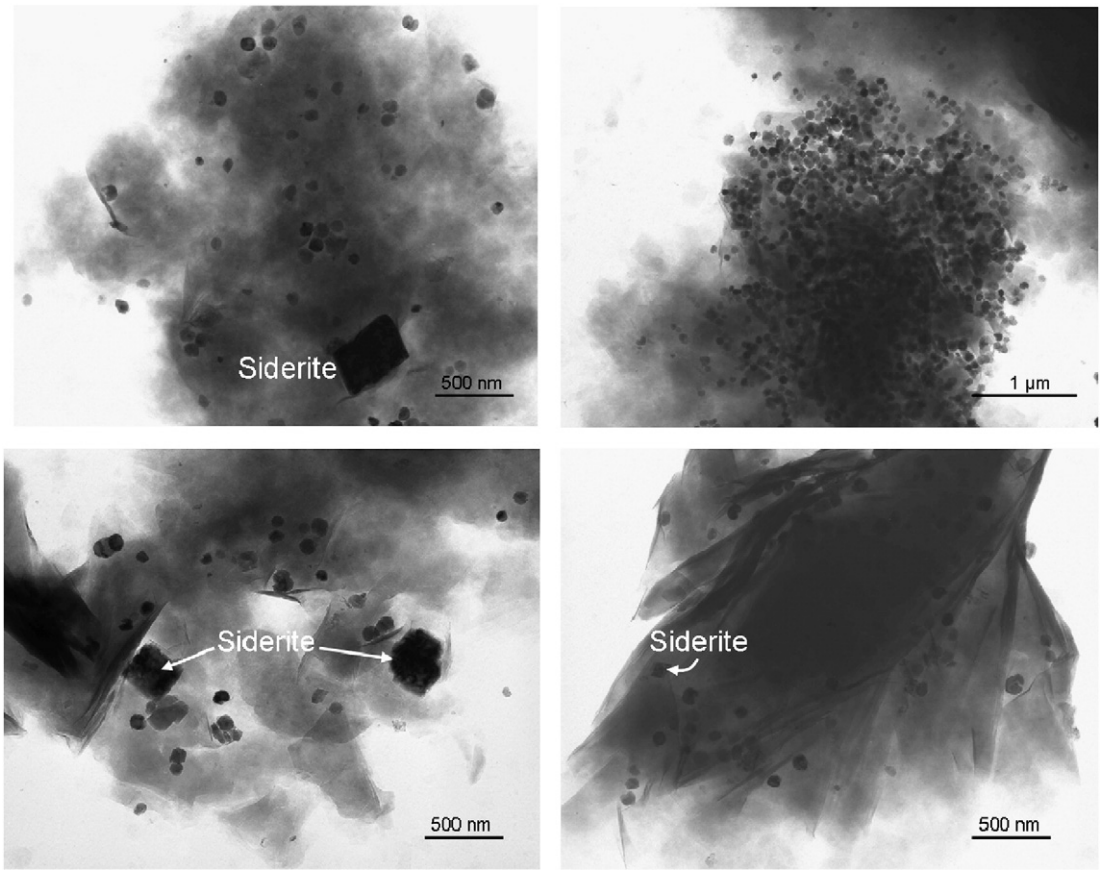

Fig. 4. TEM observations for reacted montmorillonite sample after 60 days of solid–fluid contact. Hematite–siderite coexistence on montmorillonite, with a clear dominance of hematite nanoparticles at this reaction state.

These carbonate minerals were not identified on the reacted montmorillonite after 15 and 60 days of solid–fluid interaction.

This study reveals a simplified methodology to study the reactivity of geo-materials in complex liquid–gas systems.

4. Conclusion

The main objective for this study was to understand the iron–montmorillonite–salt solution–CO_2 interactions under high gas pressure (200 bar) at 150 °C. Obviously, this study does not represent a realistic system of the hydrothermal reactivity for a clay natural barrier in contact with CO_2-rich brine solution relevant to the geological storage of CO_2. However, this simplified system can help in understanding the reaction mechanisms in more realistic experimental simulations.

Various chemical processes were characterized at the solid–fluid interfaces such as the dissolution of fine montmorillonite particles and oxidative-dissolution of elemental iron. The ionic supersaturation of interacting solution and possibly the surface complexation in the system produced the precipitation of hematite nanoparticles (<200 nm) after 15 days of reaction. The hematite nanoparticles dispersed and/or coagulated on the montmorillonite matrix caused a stable red coloration of montmorillonite composite. We assume that initially dissolved oxygen was progressively consumed in this closed-stirred system favouring the presence of divalent iron and leading to surface precipitation of iron carbonate nanocrystals (<500 nm) after 60 days

Table 3
EDS-TEM analyses in the iron carbonate nanoparticles synthesized under hydrothermal conditions.

Analysis	Mass percent for elements in iron carbonate nanoparticles							Observation
	Fe	O	C	Ni	Co	Al	Si	
Reference 1	48.20	41.42	10.36	00.00	00.00	00.00	00.00	Siderite composition
1	49.70	36.24	09.01	00.29	00.00	01.55	03.21	Reaction time: 60 days
2	48.39	37.80	08.90	00.54	00.00	01.43	02.95	Reaction time: 60 days
Average	49.04	37.02	08.95	00.41	00.00	01.49	03.08	Average composition for iron carbonate nanoparticles
Hypothetical reference 2	15.79	40.73	10.19	16.60	16.67	00.00	00.00	$FeCoNi(CO_3)_3$ solid solution
1	22.98	43.84	08.51	08.21	10.80	01.69	03.97	Reaction time: 60 days
2	14.06	44.40	09.43	16.75	14.15	00.38	00.84	Reaction time: 60 days
3	24.92	39.49	09.01	11.13	14.10	00.66	00.66	Reaction time: 60 days
4	26.95	38.86	08.51	09.84	14.03	00.77	01.01	Reaction time: 60 days
Average	22.22	41.64	08.86	11.48	13.27	00.87	01.62	Average composition for Fe–Ni –Co carbonate nanoparticles

Two types of iron carbonate were characterized, first, the iron carbonate (type siderite) and second, a complex iron–nickel–cobalt solid solution carbonate.

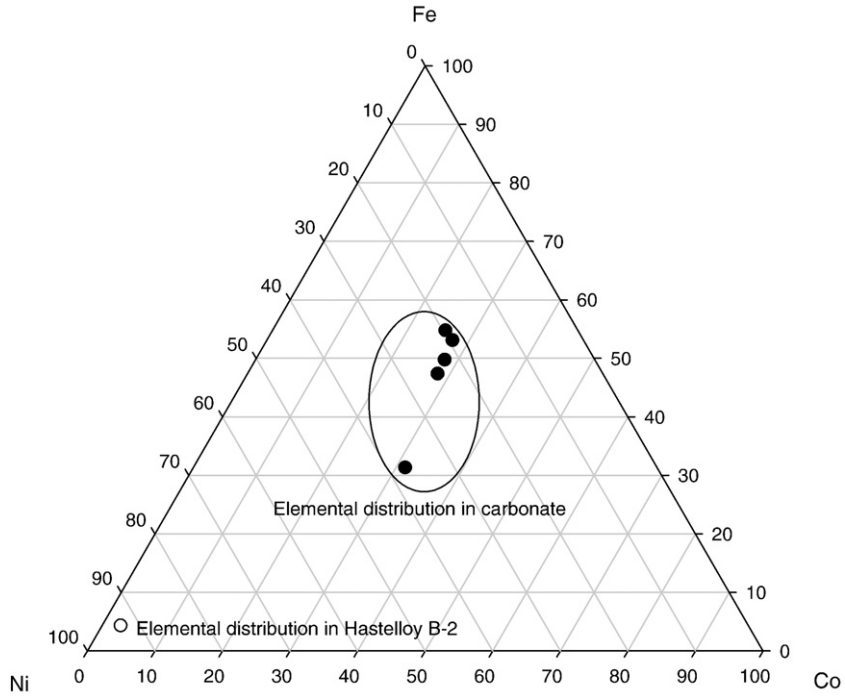

Fig. 5. The Co–Fe–Ni distribution in the Hastelloy B-2 and in the carbonates formed after 60 days of solid–fluid interaction. Micro-chemical EDS-TEM analyses.

of reaction. Thus, an atypical coexistence of hematite–iron carbonate was observed in our system. A qualitative comparison with the blank experiment (without CO_2 injection) showed clearly that the carbon dioxide increased the hydrothermal reactivity of montmorillonite because the hematite and iron carbonate formations were not observed at the same reaction times.

This study demonstrated that carbonates can be formed at high temperature and at high CO_2 pressure. This is in agreement with modelling predictions and with some experimental simulations relevant for geological storage systems, i.e. with the predicted in-situ mineral sequestration of CO_2 (Hendriks and Blok, 1993; Blunt et al., 1993; Gunter et al., 1997; Bachu, 2002; Pruess et al., 2003; Kaszuba et al., 2003; Knauss et al., 2005 and others). This experimental investigation could have important implications on the engineering practice and material science, for example on the synthesis of novel nanocomposites to be used as pigments and adsorbents.

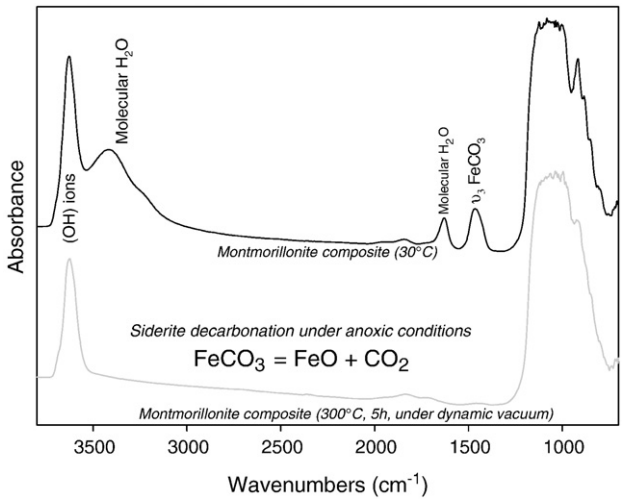

Fig. 6. Infrared measurements using an infrared microscope coupled to an environmental reaction cell. Black spectre corresponds to reacted montmorillonite sample (60 days) containing siderite (CO_3-stretching vibration band (ν_3) at 1464 cm^{-1}). Gray spectre corresponds to reacted montmorillonite sample (60 days), in-situ heated at 300 °C under dynamic vacuum for 5 h. Herein the siderite decarbonation was observed because the CO_3-stretching vibration band at 1464 cm^{-1} was removed by heating.

Acknowledgements

The authors are grateful to the National Council of Scientific Research (CNRS), France, for providing a financial grant for this work (postdoctoral position 2005–2006). This work was also supported by ANR-geocarbone (ANR-05-CO_2-006 grant) and by IMAGES program from INPL. J. Ganbaja, M. Pelletier, A. Kohler and F. Villieras are thanked for their technical and scientific help and assistance. O. Brissaud is thanked for the design and assembling of vacuum drying cell adapted on the infrared microscope. This is a G2R, UMR 7566 contribution.

References

Bachu, S., 2002. Sequestration of CO_2 in geological media in response to climate change: road map for site selection using the transform of the geological space into the CO_2 phase space. Energy Convers. Manag. 43, 87–102.

Blunt, M., Fayers, F.J., Orr, F.M., 1993. Carbon dioxide in enhanced oil recovery. Energy Convers. Manag. 34, 1197–1204.

Charlet, L., Manceau, A., 1994. Evidence for the neoformation of clays upon sorption of Co(II) and Ni(II) on silicates. Geochim. Cosmochim. Acta 58, 2577–2582.

Dickinson, S.R., Henderson, G.E., McGrath, K.M., 2002. Controlling the kinetic versus thermodynamic crystallisation of calcium carbonate. J. Cryst. Growth 244, 369–378.

Gunter, W.D., Gentzis, T., Rottenfusser, B.A., Richardson, R.J.H., 1997. Deep coalbed methane in Alberta, Canada: a fuel resource with the potential of zero greenhouse emissions. Energy Convers. Manag. 38, 217–222.

Harvey, C.O., 1943. Some notes on the calculation of molecular formula for glauconite. Am. Mineral. 28, 541–543.

Hendriks, C.A., Blok, K., 1993. Underground storage of carbon dioxide. Energy Convers. Manag. 34, 949–957.

Hochella Jr., M.F., Lower, S.K., Maurice, P.A., Penn, R.L., Sahai, N., Sparks, D.L., Twining, B.S., 2008. Nanominerals, mineral nanoparticles, and Earth systems. Science 21 (319), 1631–1635.

Kaszuba, J.P., Janecky, D.R., Snow, M.G., 2003. Carbon dioxide reaction process in a model brine aquifer at 200 °C and 200 bar: implications for geological sequestration of carbon. Appl. Geochem. 18, 1065–1080.

Knauss, K.G., Johnson, J.W., Steefel, C.I., 2005. Evaluation of the impact of CO_2, co-contaminant gas, aqueous fluid and reservoir rock interactions on the geologic sequestration of CO_2. Chem. Geol. 217, 339–350.

Lackner, K.S., Wendt, C.H., Butt, D.P., Sharp, D.H., Joyce, E.L., 1995. Carbon dioxide disposal in carbonate minerals. Energy 20, 1153–1170.

Manceau, A., Charlet, L., 1994. The mechanism of selenate adsorption on gothite and hydrous ferric oxide. J. Colloid Interf. Sci. 168, 87–93.

Montes-H, G., Marty, N., Fritz, B., Clement, A., Michau, N., 2005. Modelling of long-term diffusion-reaction in a bentonite barrier for radioactive waste confinement. Appl. Clay Sci. 30, 181–198.

Montes-Hernandez, G., Pironon, J., Villieras, F., 2006. Synthesis of a red iron oxide/montmorillonite pigment in a CO_2-rich brine solution. J. Colloid Interface Sci. 3003, 472–476.

Montes-Hernandez, G., Concha-Lozano, N., Renard, F., Quirico, E., 2009. Removal of oxyanions from synthetic wastewater via carbonation process of calcium hydroxide: Applied and fundamental aspects. J. Hazard. Mater. 166, 788–795.

Pruess, K., Xu, T., Apps, J., García, J., 2003. Numerical modeling of aquifer disposal of CO_2. SPE J. 49–60.

Seifritz, W., 1990. CO_2 disposal by means of silicates. Nature 345, 486.

Sigg, L., Behra, P., Stumm, W., 2000. Chimie des Milieux aquatiaques, 3rd Ed. Dunod, Paris.

Steefel, C.I., Van Cappellen, P.C., 1990. A new kinetic approach to modelling water-rock interactions: the role of nucleation, precursors and Ostwald ripening. Geochim. Cosmochim. Acta 54, 2657–2677.

Steefel, C.I., Van Cappellen, P.C., 1998. Reactive transport modeling of natural systems. J. Hydrol. 209, 1–7.

Wood, B.D., Radakovich, K., Golfier, F., 2007. Effective reaction at a fluid–solid interface: application to biotransformation in porous media. Adv. Water Resour. 30, 1630–1647.